Optimal sparse solution for fluorescent diffuse optical tomography: theory and phantom experimental results

Pouyan Mohajerani, Ali A. Eftekhar, Jiandong Huang, and Ali Adibi

We present a method to accurately localize small fluorescent objects within the tissue using fluorescent diffuse optical tomography (FDOT). The proposed method exploits the localized or sparse nature of the fluorophores in the tissue as *a priori* information to considerably improve the accuracy of the reconstruction of fluorophore distribution. This is accomplished by minimizing a cost function that includes the L_1 norm of the fluorophore distribution vector. Experimental results for a milk-based phantom using a fiber-based cw FDOT system demonstrate the capability of this method in accurately localizing small fluorescent objects deep in the phantom. © 2007 Optical Society of America

OCIS codes: 170.3010, 170.0170, 170.3880, 170.7050.

1. Introduction

Biological tissue is known to have low optical absorption in the near-infrared (NIR) bandwidth (700–900 nm); a property that has enabled a variety of NIR imaging techniques. Diffuse optical tomography (DOT) is a widely used method to deliver images of the optical scattering and absorption properties deep inside the tissue.[1–3] These optical properties in turn are correlated with the biological properties of the tissue.

In a typical DOT setup, the tissue is pumped with NIR light transmitted through a multiple-mode fiber, called the source fiber, which is placed on the surface of the tissue. The light scattered off the surface is then collected at different positions with many multiple-mode fibers, called detect fibers, which are connected to the optical detection devices on the other end. The propagation of light from the source fiber in the tissue can be described by a forward problem. The optical properties of the tissue are estimated by solving the inverse problem using the measurements. Two main technical challenges in DOT are the ill-posedness of the inverse problem and the relatively modest contrast between the optical properties of healthy and abnormal tissues.[1] The former problem can be mitigated utilizing *a priori* information about the optical properties of the tissue under investigation. Such information is often obtained from other imaging techniques, such as magnetic resonance imaging (MRI) and x-ray imaging.[4]

The low contrast between healthy and abnormal tissues can be increased by the administration of fluorescent contrast agents and molecular probes that target specific cells.[5–8] Fluorescent diffuse optical tomography (FDOT) seeks to estimate the spatial distribution of the concentration or lifetime of exogenous and endogenous fluorophores in tissue using surface optical measurements[9–16] and has diverse applications such as early cancer detection[17,18] and monitoring and optimization of photodynamic therapy.[19] The fluorescent contrast agents are often localized in certain areas of interest, e.g., cancerous lesions, rather than smoothly distributed within the tissue. Localization of such fluorescent objects embedded in phantoms and tissues has been the subject of many studies.[20–26] Detection of small isolated objects in bulk tissue, deemed as a "stumbling block" of optical methods for tumor detection,[27] can be specially improved using such target-specific contrast agents.

Here we show how the localized pattern, or sparseness, of fluorophores in tissues can be exploited as *a priori* information to improve the resolution of FDOT systems. The proposed method relies on a small number of measurements to rapidly localize small fluorescent objects in a large volume of highly scattering tissue. The main underlying assumption is that the

The authors are with the Department of Electrical and Computer Engineering, Georgia Institute of Technology, 777 Atlantic Drive Northwest, Atlanta, Georgia 30332. A. Adibi's e-mail address is adibi@ece.gatech.edu.

Received 5 July 2006; revised 30 November 2006; accepted 1 December 2006; posted 5 December 2006 (Doc. ID 72652); published 13 March 2007.

0003-6935/07/101679-07$15.00/0

fluorophores are localized in small volumes or, in other words, in a sparse pattern. This is specially the case in the early stages of cancer where the size of cancerous tumors tagged with the fluorescent probes is small compared with the resolution of DOT.

The work presented in this paper is developed in the context of frequency-domain FDOT.[28,29] Using a milk-based phantom, experimental results are obtained from a fiber-based cw FDOT system. The proposed approach is able to effectively reconstruct the two small fluorescent objects used in this experiment. The result of a conventional reconstruction method is also presented for comparison purposes.

We first present the mathematical framework of FDOT in Section 2. In Section 3 we present our approach for solving the inverse problem in FDOT based on the sparseness of the fluorophore distribution. The design and technical details of our FDOT system are discussed in Section 4. The experimental results are presented in Section 5, and Section 6 contains a discussion about the advantages and shortcomings of the presented approach. Final conclusions are summarized in Section 7.

2. System Modeling of Fluorescent Diffuse Optical Tomography

The problem of finding the fluorophore distribution within the tissue (i.e., the inverse problem) based on emission measurements, can be modeled as a linear problem. As the first step in establishing such a relation, we need to model the propagation of the excitation (or pump) light and the emission light in the tissue, or in other words, solve the forward problem. The propagation of light in tissue is governed by the radiative transfer equation that can be approximated by the diffusion approximation (DA).[1] The boundary conditions required to solve the equations formed by the DA are determined based on the medium neighboring the tissue. The two main types of surrounding media are air and perfectly absorbing medium. The Robin boundary condition is used for tissue–air interfaces and the light fluence is forced to zero where tissue is surrounded by a perfectly absorbing medium.[30] The finite-element method (FEM) is usually the method of choice for solving the equations formed by the DA.[31]

We are concerned with estimating the fluorophore distribution in the tissue (or phantom) and not the spatial distribution of the optical properties. Therefore, we assume these optical properties are known *a priori*. Estimations of the optical properties of the tissue can be obtained using various DOT techniques prior to FDOT measurements.[9]

The fluorophore distribution in the tissue can be represented by a $K \times 1$ vector X, where K is the number of nodes in the 3D FEM mesh. Each element of X denotes the fluorophore concentration on the corresponding mesh node. The relationship between X and the optical measurements gathered on the surface of the tissue can be derived in a few steps.

First, we introduce the FEM formulation describing the propagation of the excitation light and the emission light in the tissue. Let N_s and N_d denote the number of source and detector fibers placed on the tissue surface. The relation between fluences and source terms in the tissue can be written as

$$K_e \Phi_e^{(i)} = Q_e^{(i)}, \tag{1}$$

$$K_m \Phi_m^{(i)} = Q_m^{(i)}, \tag{2}$$

where $\Phi_m^{(i)}$ ($\Phi_e^{(i)}$) and $Q_m^{(i)}$ ($Q_e^{(i)}$) are fluence and source vectors at the emission (excitation) wavelength, respectively, when the ith source fiber is used. Here we assume that only one source fiber is excited at a time. The complex matrix K_m (K_e) is the stiffness matrix obtained from the FEM formulation at the emission (excitation) wavelength.[9] The excitation source vector, $Q_e^{(i)}$, is nonzero only on the mesh nodes that neighbor the ith source fiber. The emission source vector, $Q_m^{(i)}$, is derived as follows. Note that each mesh node acts as a light source at the emission wavelength. The $K \times 1$ vector, $Q_m^{(i)}$, represents the intensities of these sources. This vector, as seen in Eq. (2), is actually the source vector in the FEM formulation of the forward problem at the emission wavelength. The intensity of each mesh node as a fluorescent source is clearly equal to the concentration of fluorophores on that node multiplied by the amount of excitation light that reaches that node, namely, the excitation fluence at that node. Therefore we have

$$Q_m^{(i)} = \mathrm{diag}\left[\Phi_e^{(i)}\right] X, \tag{3}$$

where for any $K \times 1$ vector g, $\mathrm{diag}(g)$ is defined as a $K \times K$ diagonal matrix V with the elements of V as its main diagonal elements. Furthermore, we need to describe the measurements in terms of the FEM model parameters. Let $M^{(i)}$ be an $N_d \times 1$ complex vector representing the emission measurements at all detector fibers when the tissue is excited by the ith source fiber. Generally, we can write

$$M^{(i)} = C \Phi_m^{(i)}, \tag{4}$$

where C is an $N_d \times K$ real matrix describing measurements obtained on each detector fiber as a linear combination of the fluences of its neighboring nodes.[32]

The last step in establishing the relation between measurements M and the desired unknown vector X involves inserting Eqs. (1), (2), and (3) into Eq. (4), which results in a set of N_s equations:

$$M^{(i)} = C K_m^{-1} \mathrm{diag}\left[K_e^{-1} Q_e^{(i)}\right] X. \tag{5}$$

Stacking all the measurements for all the sources in an $N_s N_d \times 1$ column vector M yields the following linear equation:

$$M = ZX + F, \tag{6}$$

where F is a complex $N_s N_d \times 1$ column vector representing additive measurement noise and

$$M = \begin{bmatrix} M^{(1)} \\ \vdots \\ M^{(N_s)} \end{bmatrix}, \qquad Z = \begin{bmatrix} CK_m^{-1}\,\mathrm{diag}\left(K_e^{-1}Q_e^{(1)}\right) \\ \vdots \\ CK_m^{-1}\,\mathrm{diag}\left(K_e^{-1}Q_e^{(N_s)}\right) \end{bmatrix}. \quad (7)$$

Equation (6) is the final equation that relates the unknown fluorophore distribution X to the measurements M. Note that we do not need to actually carry matrix inversions in Eqs. (5) and (7). Instead, we use Gaussian elimination, which significantly reduces the computational complexity. The inverse problem of FDOT consists of solving Eq. (6) for X given M and Z. It should be noted that, as the number of FEM nodes is often much more than the number of measurements, Eq. (6) is a highly underdetermined problem.

3. Proposed Approach

A. Sparse Solutions to Underdetermined Linear Problems

The problem of finding the sparsest solution, namely, one with the smallest number of nonzero elements, to an underdetermined problem is an interesting one with diverse applications. A powerful mathematical fact is that, under certain conditions, the solution with the minimum L_1 norm is often the sparsest solution as well.[33] The L_1 and L_2 norms of an arbitrary vector v, with elements $v(i)$, are denoted as $\|v\|_1$ and $\|v\|_2$, respectively, and defined as $\|v\|_1 = \sum |v(i)|$ and $\|v\|_2 = (\sum |v(i)|^2)^{1/2}$. To clarify the rationale behind this fact, consider the simple case of a linear equation with two unknowns. Specifically, suppose we want to find the sparsest solution of the equation $1.5x_1 + x_2 = 1$. Figure 1 shows the solution line that includes all the possible solutions of this equation. The dotted lines and the dotted circles in Fig. 1 denote the contours of functions $l_1(x_1, x_2) = |x_1| + |x_2|$ and $l_2(x_1, x_2) = (x_1^2 + x_2^2)^{1/2}$, respectively, i.e., the contours of points with constant L_1 and L_2 norms.

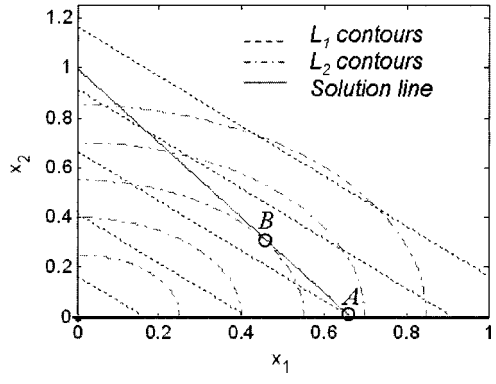

Fig. 1. Solution line for equation $1.5x_1 + x_2 = 1$ and contours of the L_1 and L_2 norms. Points A and B denote the points on the solution line (solid line) with minimum L_1 and L_2 norms, respectively. Point A is the sparsest solution, as it has only one nonzero coordinate, and point B is not a sparse solution, since all its coordinates are nonzero.

For this example, the solution with the least L_1 norm can be found by finding the closest dotted line to the origin that crosses the solution line, which is point A in Fig. 1. As seen, point A lies on the x_1 axis. This means that the solution with the least L_1 norm has only one nonzero element, i.e., is the sparsest. Point B in Fig. 1 is the solution with the least L_2 norm, which is obviously not sparse.

B. Sparseness of Fluorophore Distribution and the Effect of Background Fluorescence

The fluorescent objects formed in the tissue through selective uptake of probe fluorophores are often fairly small. For example, when tagged with fluorescent probes, the tumors in the early stage of cancer can form fluorescent objects as small as 0.5 cm^3.[21] These small fluorescent objects are often modeled as fluorescent point sources within the tissue.[22,34] Reference 35 employs an FDOT system with reflection geometry to verify that a point-source model often sufficiently represents tumors smaller than 1 cm^3 in size, as the optical measurements obtained for tumors with different sizes (0.2 to 1 cm in diameter) show similar intensity profiles.

Background fluorescence is often present because of the exogenous fluorophores not uptaken by targeted lesions and the autofluorescence of tissue.[36] The effect of such background emission on the measurements, even for high uptake ratios, can be significant.[34] Various methods have been proposed for removal or subtraction of the background fluorescence prior to the processing of the FDOT measurements.[36,37] Other approaches account for background fluorescence by applying bound constraints on the fluorophore concentration values in the optimization algorithm.[38] Removal of the background fluorescence often results in the perfect uptake scenario,[11] where the fluorophores are assumed to exist only in the fluorescent inclusions.

We first obtain an estimate of the background fluorescence as described in Section 4 and then subtract it from the emission measurements. Therefore, we can assume perfect or very high uptake of fluorophores by targeted lesions. This assumption, together with the fact that the fluorescent inclusions are generally small, implies that only a few elements of vector X have significant values and the rest are either zero or have a minor effect on the measurements. In other words, fluorophore distribution X can be reasonably considered sparse when the fluorophores are mainly concentrated in small lesions and the background fluorescence is largely removed.

Finally, since the autofluorescence emission is generally distributed smoothly over the tissue volume, it can be modeled with few parameters that can be added to the problem unknowns.[36] Such modeling of the autofluorescence preserves the sparseness of the unknown vector. The details of this method for background emission reduction will be presented elsewhere.[39]

C. Proposed Approach Toward the Inverse Problem in Fluorescent Diffuse Optical Tomography

We demonstrate our approach for finding the sparsest solution to the inverse problem in FDOT, using the idea discussed in Subsection 3.A. We achieve this by minimizing a cost function based on the weighted addition of the L_1 norm of the solution and the mismatch between the measurements and the system model. Specifically, the desired solution, X_1, can be written as

$$X_1 = \arg\min_{X \geq 0} \{f_1(X) = \|M - ZX\|_2^2 + \alpha \|X\|_1\}, \quad (8)$$

where α is the weighting constant balancing the weight of the two contributing terms. We assume the measurement noise in the system can be modeled by a vector of independent identically distributed Gaussian variables, and therefore do not apply any weighting to the data fidelity term in Eq. (8). In a system limited by the detector shot noise, the data fidelity term should be properly weighted by the inverse of the noise covariance matrix.[9] Note that the nonnegativity constraint is imposed as the fluorophore concentration cannot be negative. The convex cost function, f_1, can be minimized using various convex optimization techniques. Also, due to the positivity constraint, we can replace $\|X\|_1$ by $\sum_i X(i)$ in Eq. (8) and arrive at a differentiable and convex cost function that can be minimized using quadratic programming techniques. A preconditioning method is used to improve the performance of the above approach by normalizing the columns of matrix Z defined in Eq. (7). This normalization compensates for the low level of emission light coming from nodes deep in the tissue. Specifically, we used a diagonal matrix W, defined in Eq. (11), to normalize each column of matrix Z to norm 1. The resultant preconditioned system matrix is therefore given as ZW. The preconditioned problem is rewritten as

$$X_1 = WY_1, \quad (9)$$

$$Y_1 = \arg\min_{Y > 0} \{f_1(Y) = \|M - ZWY\|_2^2 + \alpha \|Y\|_1\}, \quad (10)$$

$$W(i, j) = \begin{cases} \|Z_i\|_2^{-1} & i = j \\ 0 & i \neq j \end{cases}, \quad i, j = 1, \ldots, K, \quad (11)$$

where Z_i is the ith column of Z.

4. Fluorescent Diffuse Optical Tomography Experimental Setup

We delineate the design and specifications of our cw FDOT system to verify our theoretical approach. Since a cw FDOT system is a special case of frequency-domain FDOT systems, the formulations and methods presented so far are applicable here as well. The schematic of this system is depicted in Fig. 2. The phantom used in the experiment consists of a cylinder with a diameter of 7.5 cm and height of 6 cm, which is filled with a milk-based solution. The interior of the cylinder is painted black to realize a perfectly absorbing boundary condition.[30] The top surface of the cylinder is open and in direct contact with air. The cylinder is filled with diluted milk and Indian ink solution. Milk is known to have similar scattering properties as tissue and the Indian ink is added to increase the absorption of the solution.[40] Both detector and source fibers are placed on the top surface of the phantom. This measurement geometry (reflection geometry) is used to emulate real measurements on tissue where only one side of the tissue is accessible for measurement, such as in breast imaging. The phantom is assumed to have homogeneous optical properties.

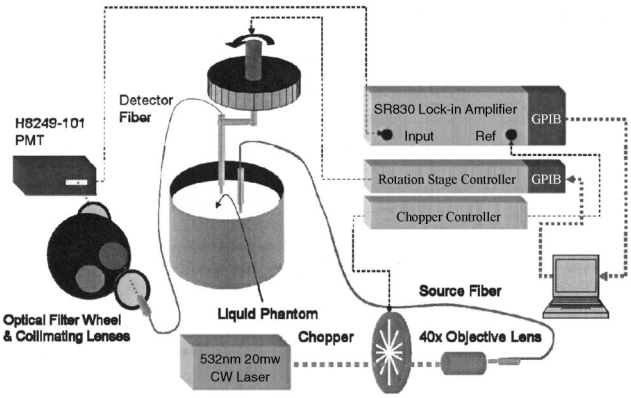

Fig. 2. Schematic of the fiber-based cw FDOT setup. The surface measurements are collected via the multimode fiber and detected using the PMT after going through a filter to separate the emitted light from the excitation (pump) light. The lock-in technique allows for a high SNR in the emission measurements.

Small glass cuvettes filled with Rhodamine 6G (dissolved in methanol), used as small fluorescent objects, are fixed inside the liquid phantom using very thin metallic strings. The effect of these metallic strings on light propagation in the phantom is negligible. To improve the signal-to-noise ratio (SNR) of measurements, we employ the lock-in technique in our experiments. A cw solid-state laser source at wavelength 532 nm is modulated by a mechanical chopper at a frequency of 2 kHz and is coupled into a 600 μm core multiple-mode fiber using a 40$\times$ objective lens. Note that although a clinical DOT system would usually use a NIR laser source (as the blood hemoglobin makes the tissue highly absorbing in shorter wavelengths),[1] the use of Rhodamine 6G as a visible wavelength dye is optional for experimental verification due to its high quantum yield.[11] However, the optical characteristics of the phantom (i.e., scattering and absorption cross section) at 532 nm are similar to those of the real tissue at NIR wavelength. Furthermore, since the modulation frequency is very small, the system behaves essentially like a cw DOT system.

The excitation light is delivered to the surface of the liquid phantom using the multimode source fiber. This light excites the fluorophores in the phantom. The ex-

citation light and the emission light are collected at the liquid surface using a multimode detector fiber with a core diameter of 600 μm. The detector fiber is attached to a computer-controlled rotation stage, which scans the detector fiber around a circle across the top surface of the phantom. The measurements are taken on a set of equally spaced angles around this circle.

The excitation light and the emission light collected by the detector fiber are separated using two bandpass filters mounted on a filter wheel, as shown in Fig. 2. A Hamamatsu H8249-101 photomultiplier tube (PMT) module is used as the detector and the output of the PMT is connected to the input port of the lock-in amplifier, which measures the relative intensity and phase shift of the detected signal. Due to the very low modulation frequency of this experiment, the phase of the detected signal has very small variations for different positions of the detector fiber. The signal detected using the lock-in amplifier has a much higher SNR than the signal detected by direct power measurement. A general-purpose interface bus module is used to acquire data from the lock-in amplifier and control the rotation stage. The measurements obtained from the lock-in amplifier are then used to find the fluorophore distribution within the tissue using the approach presented in Subsection 3.C. The phantom shows significant background emission due to the autofluorescence of milk.[41] As suggested in Subsection 3.B, we adopt a subtraction scheme to remove the autofluorescence of the phantom from the measurements prior to processing. We remove the autofluorescence signal in a differential manner. That is, we first obtain emission measurements of the phantom before the insertion of fluorescent objects and then subtract them from the measurements acquired after insertions of the objects.

We use the method proposed in Ref. 42 for measuring the absorption coefficient (μ_a) and the scattering coefficient (μ_s) of the phantom solution. In this method, infinite medium measurements (emulated using a large tank) are used to estimate μ_a and μ_s of the solution for different concentrations of milk and ink. The absorption coefficient of ink is obtained using the transmission method (assuming negligible scattering for ink).

5. Experimental Results

The cw DOT system described above is used to experimentally observe and validate the merit of the approach presented in Subsection 3.C. Figure 3 shows the configuration of this experiment. The large cylinder represents the cylinder that is filled with diluted milk and India ink solution (as described in Section 4). Two small glass cuvettes with approximate dimensions of 1 mm × 1 mm × 3 mm filled with Rhodamine 6G are placed inside the liquid phantom at locations marked with squares in Fig. 3. The two glass cuvettes are placed 1 cm under the phantom surface and are approximately 2 cm apart. The dye solution has a concentration of 417 μM, therefore, each cuvette contains approximately 1.25 nmol of Rhodamine 6G. The phantom is a 260 ml solution of

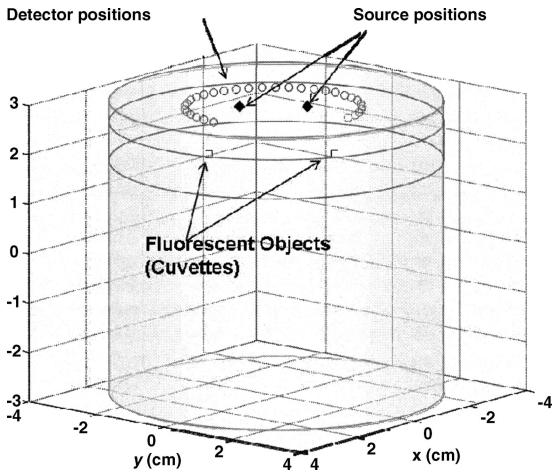

Fig. 3. Configuration of the experiment. The large cylinder denotes the phantom. The source position and detector positions are depicted on the top of the phantom. Two squares show the locations of the small fluorescent objects (i.e., cuvettes). The smaller cylinder shown as the upper portion of the phantom depicts the optimization domain for which the inverse problem is solved.

25% water and 75% whole milk. India ink (waterproof drawing ink from Higgins) with a concentration of 12.5 ppm is added to the solution to increase absorption. The optical properties, μ_a and μ_s, of this solution are estimated at both the excitation wavelength (532 nm) and the emission bandwidth (580–620 nm), as described in Section 4, and are presented in Table 1. The source and detector fibers are placed at the top circle of the cylinder and measurements are acquired for 30 equally spaced angles, as shown in Fig. 3. To calculate the forward model for the phantom, a 3D FEM mesh of 33,750 nodes and 186,345 tetrahedral elements is used to discretize the phantom volume. The emission light and the excitation light are separated using two bandpass filters. A convex optimization technique is used to solve the inverse problem. To reduce the computational complexity, the optimization domain is limited to a smaller cylinder with a height of 1 cm, shown as the upper portion of the larger cylinder in Fig. 3.

To calculate the distribution of the fluorophores the inverse problem is solved using the approach presented in Subsection 3.C. Figure 4(a) shows the fluorophore distribution estimated from the emission measurements using the proposed method. The fluorophore distribution is depicted using horizontal cross sections at different z coordinates for 1.5 cm

Table 1. Optical Properties of the Phantom Solution

Wavelength	μ_a of the 75% Milk Solution (cm^{-1})	μ_s of Phantom (cm^{-1})	μ_a of Phantom (cm^{-1})
Excitation (532 nm)	0.0088	20.06	0.035
Emission (580–620 nm)	0.0083	12.15	0.033

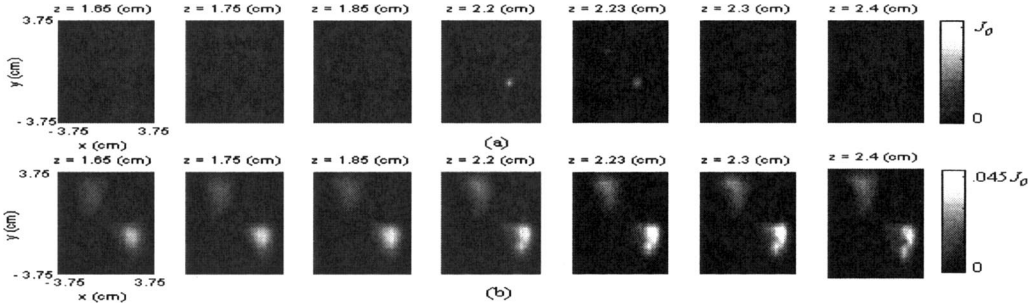

Fig. 4. (a) and (b) Fluorophore concentrations reconstructed using our approach and a Tikhonov-based approach, respectively. The axes (x, y, z) correspond to the spatial coordinates of the cylindrical phantom.

$< z < 2.5$ cm, where the estimated distribution has nonzero values. The proposed method has been able to find the positions of the two fluorescent cuvettes (as seen in the cross sections with the corresponding z coordinates) with fairly good accuracy. For comparison purposes, we also used a conventional method based on the Tikhonov regularizer[26] for solving the inverse problem. The solution obtained using the Tikhonov-based method is shown in Fig. 4(b). As seen, the solution is expectedly highly spread out along the three spatial coordinates.

6. Discussion

Localization of the fluorescent probes in a large tissue is a challenging problem due to a very large degree of freedom (DOF), i.e., the number of unknown variables. The large number of independent measurements required for this task implies a long acquisition time. In many cases, such localization may even be impossible due to the restricted and ill-posed measurement geometry. The method proposed in this paper takes advantage of the sparseness of the fluorophore distribution to localize isolated fluorescent objects in the tissue using a small set of measurements. There is an upper limit on the maximum number of fluorescent objects in the tissue that can be resolved properly using this method. This upper limit is a function of the total number of measurements and the DOF (a lower bound for this limit is discussed in Ref. 31 for a general linear problem). We have considered a sparse model for the distribution of fluorophores in tissue. This assumption is justified in many important cases where the targeted regions form small fluorescent objects (with sizes of the order of 0.5 cm^3) when tagged with fluorescent probes. However, there are clearly situations where the size of the fluorescent inclusions in tissue is too large to fit a sparse model, for example, as in the case of metastatic spread of cancer (though Ref. 19 argues that these metastatic lesions can also be mimicked by multiple small targets).

The main optimization problem in both the conventional and our method is based on a convex cost function. A nonnegative convex optimization technique can therefore be used to find the optimal solution for both methods. However, since the Hessian matrix of the cost function in the proposed method is only semipositive definite and not absolutely positive definite, the optimization has a slightly higher computation cost compared to the Tikhonov-based approach where the Hessian matrix of the cost function is positive definite. To assure the convergence of the convex optimizer in a reasonable time, we need to maintain a low DOF. We have reduced the DOF by limiting the optimization domain to a portion of the whole tissue. Furthermore, we use a fine mesh for solving the forward problem and a courser mesh with a fewer number of nodes for the inverse problem. The number of optimization DOFs used in this work is 5381.

As observed, an accurate solution is obtained by as low as 60 measurements. Since all these measurements are obtained for only two source positions, the measurements can be potentially accomplished in two single-shot acquisitions, allowing a very low data acquisition time. It should also be mentioned that, although our experimental results are presented for a cw FDOT system at 532 nm, results are easily extendable for NIR FDOT systems working at high modulation frequencies.

7. Conclusion

We have presented a new approach to fluorescent diffuse optical tomography based on a sparse model for distribution of the fluorescent probes in the tissue with considerably better accuracy than the conventional technique. Utilizing the sparse model of fluorophore distribution and minimizing its L_1 norm enable the FDOT systems to gain higher spatial resolution with a smaller number of measurements. The experimental results on tissue phantom agree with the theory and verify the effectiveness of the proposed method and its advantage over the conventional method.

References and Notes

1. A. P. Gibson, J. C. Hebden, and S. R. Arridge, "Recent advances in diffuse optical imaging," Phys. Med. Biol. **50,** 1–43 (2005).
2. V. Ntziachristos, A. H. Hielscher, A. G. Yodh, and B. Chance, "Diffuse optical tomography of highly heterogeneous media," IEEE Trans. Med. Imaging **20,** 470–478 (2001).
3. A. H. Hielscher, A. Y. Bluestone, G. S. Abdoulaev, A. D. Klose, J. Lasker, M. Stewart, U. Netz, and J. Beuthan, "Near-infrared diffuse optical tomography," Dis. Markers **18,** 313–337 (2002).
4. M. Guven, B. Yazici, X. Intes, and B. Chance, "Diffuse optical

tomography with *a priori* anatomical information," Phys. Med. Biol. **50,** 2837–2858 (2005).
5. K. Licha, "Contrast agents for optical imaging," Top. Curr. Chem. **222,** 1–29 (2002).
6. J. V. Frangioni, "*In vivo* near-infrared fluorescence imaging," Curr. Opin. Chem. Biol. **7,** 626–634 (2003).
7. E. M. Sevick-Muraca, J. P. Houston, and M. Gurfinkel, "Fluorescence-enhanced, near infrared diagnostic imaging with contrast agents," Curr. Opin. Chem. Biol. **6,** 642–650 (2002).
8. R. J. Gillies, "*In vivo* molecular imaging," J. Cell. Biochem. **87,** 231–238 (2002).
9. A. B. Milstein, S. Oh, K. J. Webb, C. A. Bouman, Q. Zhang, D. A. Boas, and R. P. Milane, "Fluorescence optical diffusion tomography," Appl. Opt. **42,** 3081–3094 (2003).
10. V. Ntziachristos, C. Bremer, E. E. Graves, J. Ripoll, and R. Weissleder, "*In vivo* tomographic imaging of near-infrared fluorescent probes," Mol. Imaging **1,** 82–88 (2002).
11. A. Godavarty, M. J. Eppstein, C. Zhang, S. Theru, A. B. Thompson, M. Gurfinkel, and E. M. Sevick-Muraca, "Fluorescence-enhanced optical imaging in large tissue volumes using a gain modulated ICCD camera," Phys. Med. Biol. **48,** 1701–1720 (2003).
12. G. Zacharakis, J. Ripoll, and V. Ntziachristos, "Fluorescent protein tomography scanner for small animal imaging," IEEE Trans. Med. Imaging **24,** 878–885 (2005).
13. A. Cong and G. Wang, "A finite-element-based reconstruction method for 3D fluorescence tomography," Opt. Express **13,** 9847–9857 (2005).
14. J. H. Chang, H. L. Graber, and R. L. Barbour, "Imaging of fluorescence in highly scattering media," IEEE Trans. Biomed. Eng. **44,** 810–822 (1997).
15. M. A. O'Leary, D. A. Boas, X. D. Li, B. Chance, and A. G. Yodh, "Fluorescence lifetime imaging in turbid media," Opt. Lett. **21,** 158–160 (1996).
16. X. D. Li, M. A. O'Leary, D. A. Boas, B. Chance, and A. G. Yodh, "Fluorescent diffuse photon density waves in homogeneous and heterogeneous turbid media: analytic solutions and applications," Appl. Opt. **35,** 3746–3758 (1996).
17. V. Ntziachristos, C. Bremer, E. E. Graves, J. Ripoll, and R. Weissleder, "*In vivo* tomographic imaging of near-infrared fluorescent probes," Mol. Imaging **1,** 82–88 (2002).
18. E. M. Sevick-Muraca, "Fluorescence-enhanced optical imaging and tomography for cancer diagnostics," in *Proceedings of IEEE International Symposium on Biomedical Imaging* (IEEE, 2004), pp. 1482–1485.
19. W. B. Pogue and T. Hasan, "Targeting in photodynamic therapy and photo-imaging," Opt. Photon. News **14,** 36–43 (2003).
20. C. D' Andrea, L. Spinelli, D. Comelli, G. Valentini, and R. Cubeddu, "Localization and quantification of fluorescent inclusions embedded in turbid media," Phys. Med. Biol. **50,** 2313–2327 (2005).
21. R. Roy, A. Godavarty, and E. M. Sevick-Muraca, "Fluorescence-enhanced optical tomography of a large tissue phantom using point illumination geometries," J. Biomed. Opt. **11,** 044007 (2006).
22. E. L. Hull, M. G. Nichols, and T. H. Foster, "Localization of luminescent inhomogeneities in turbid media with spatially resolved measurements of cw diffuse luminescence emittance," Appl. Opt. **37,** 2755–2765 (1998).
23. M. A. O'Leary, D. A. Boas, B. Chance, and A. G. Yodh, "Reradiation and imaging of diffuse photon density waves using fluorescent inhomogeneities," J. Lumin. **60,** 281–268 (1994).
24. M. Alrubaiee, M. Xu, S. K. Gayen, and R. R. Alfano, "Localization and cross section reconstruction of fluorescent targets in *ex vivo* breast tissue using independent component analysis," Appl. Phys. Lett. **89,** 133902 (2006).
25. A. Eidsath, V. Chernomordik, A. Gandjbakhche, P. Smith, and A. Russo, "Three-dimensional localization of fluorescent masses deeply embedded in tissue," Phys. Med. Biol. **47,** 4079–4092 (2002).
26. Y. Chen, G. Zheng, Z. H. Zhang, D. Blessington, M. Zhang, H. Li, Q. Liu, L. Zhou, X. Intes, S. Achilefu, and B. Chance, "Metabolism-enhanced tumor localization by fluorescence imaging: *in vivo* animal studies," Opt. Lett. **28,** 2070–2072 (2003).
27. B. Chance, K. Kang, L. He, H. Liu, and S. Zhou, "Precision localization of hidden absorbers in body tissues with phase-array optical systems," Rev. Sci. Instrum. **67,** 4324–4332 (1996).
28. H. Jiang, "Frequency-domain fluorescent diffusion tomography: a finite-element-based algorithm and simulations," Appl. Opt. **37,** 5337–5343 (1998).
29. B. Pogue, M. Testorf, T. McBride, U. Osterberg, and K. Paulsen, "Instrumentation and design of a frequency-domain diffuse optical tomography imager for breast cancer detection," Opt. Express **1,** 391–403 (1997).
30. S. R. Arridge, M. Schweiger, M. Hiraoka, and D. T. Delpy, "The finite element method for the propagation of light in scattering media: boundary and source conditions," Phys. Med. Biol. **22,** 1779–1792 (1995).
31. S. R. Arridge, M. Schweiger, M. Hiraoka, and D. T. Delpy, "A finite element approach for modeling photon transport in tissue," Phys. Med. Biol. **20,** 299–309 (1993).
32. S. R. Arridge, J. P. Kaipio, V. Kolehmainen, M. Schweiger, E. Somersalo, T. Tarvainen, and M. Vauhkonen, "Approximation errors and model reduction with an application in optical diffusion tomography," Inverse Probl. **22,** 175–195 (2006).
33. S. S. Chen, D. L. Donoho, and M. A. Saunders, "Atomic decomposition by basis pursuit," SIAM (Soc. Ind. Appl. Math.) Rev. **43,** 129–159 (2001).
34. J. Wu, Y. Wang, L. Perelman, I. Itzkan, I. Ramachandra, R. Dasari, and M. S. Feld, "Time-resolved multichannel imaging of fluorescent objects embedded in turbid media," Opt. Lett. **20,** 489–491 (1995).
35. A. B. Milstein, "Imaging of near-infrared fluorescence, absorption, and scattering in turbid media," Ph.D. dissertation (Purdue University, West Lafayette, Ind., 2004).
36. A. Soubret and V. Ntziachristos, "Fluorescence molecular tomography in the presence of background fluorescence," Phys. Med. Biol. **51,** 3983–4001 (2006).
37. M. Gao, G. Lewis, G. M. Turner, A. Soubret, and V. Ntziachristos, "Effects of background fluorescence in fluorescence molecular tomography," Appl. Opt. **44,** 5468–5474 (2005).
38. J. H. Chang, H. L. Graber, and R. L. Barbour, "Improved reconstruction algorithm for luminescence optical tomography when background lumiphore is present," Appl. Opt. **37,** 3547–3552 (1998).
39. P. Mohajerani (Department of Electrical and Computer Engineering, Georgia Institute of Technology, 777 Atlantic Station, N.W., Atlanta, GA, 30332). A. A. Eftekhar, and A. Adibi are preparing a manuscript to be called "Localization of small fluorescent objects in tissue in the presence of diffuse background fluorescence."
40. M. D. Waterworth, B. J. Joblin, T. van Doorn, and H. E. Niesler, "Optical transmission properties of homogenised milk used as a phantom material in visible wavelength imaging," Aust. Phys. Eng. Sci. Med. **18,** 39–44 (1995).
41. J. Christensen, L. Norgaard, R. Bro, and S. B. Engelsen, "Multivariate autofluorescence of intact food systems," Chem. Rev. **106,** 1979–1994 (2006).
42. L. S. Zhang, L. Zhang, C. P. Zhang, S. W. Qi, T. Xu, and J. G. Tian, "Measurements of absorption and anisotropy coefficients of the fat emulsion intralipid-10%," Chin. Phys. Lett. **21,** 2517–2520 (2004).